Measurements of the edge current evolution and comparison with neoclassical calculations during MAST H-modes using motional Stark effect

Plasma Phys. Control. Fusion **54** (2012) 025001 (8pp) doi:10.1088/0741-3335/54/2/025001

Measurements of the edge current evolution and comparison with neoclassical calculations during MAST H-modes using motional Stark effect

M F M De Bock[1], J Citrin[2], S Saarelma[3], D Temple[3], N J Conway[3], A Kirk[3], H Meyer[3], C A Michael[3] and the MAST team

[1] Eindhoven University of Technology, PO Box 513, 5600 MB Eindhoven, The Netherlands
[2] FOM-Institute for Plasma Physics Rijnhuizen, EURATOM/FOM Association, PO Box 1207, 3430 BE, Nieuwegein, The Netherlands
[3] EURATOM/CCFE Fusion Association, Culham Science Centre, Abingdon, OX14 3DB, UK

Received 29 August 2011, in final form 14 November 2011
Published 5 January 2012
Online at stacks.iop.org/PPCF/54/025001

Abstract
Edge localized modes (ELMs), that are present in most tokamak H- (high confinement) modes, can cause significant damage to plasma facing components in fusion reactors. Controlling ELMs is considered necessary and hence it is vital to understand the underlying physics. The stability of ELMs is typically expressed in terms of the pressure gradient ∇p in the edge and the edge current density j_ϕ. Both ∇p and j_ϕ are usually derived from profiles fitted to the measured edge density and temperature profiles, where for the calculation of j_ϕ neoclassical theory is used.

This paper presents direct measurements of the magnetic pitch angle γ_m evolution in the edge and the derived j_ϕ. These provide a method to validate the j_ϕ as derived with neoclassical theory and they open up the possibility to find a complete, self-consistent set of edge profiles, that fit density, temperature and γ_m measurements, hence allowing for a more accurate stability analysis.

(Some figures may appear in colour only in the online journal)

1. Introduction

The intermittent energy loss caused by edge localized mode (ELM) instabilities will cause unacceptable damage to divertor materials in burning plasma fusion reactors such as ITER and beyond. Several techniques are investigated to suppress or control ELMs, and for this understanding ELM stability is required [1, 2]. Together with the edge pressure gradient ∇p, the stability with respect to ELMs is determined by the edge current density j_ϕ.

Typically j_ϕ is calculated using neoclassical theory, with the bootstrap current being the dominant contribution in the plasma edge [3, 4]. This calculation relies on the profiles of ion and electron temperatures (T_i, T_e) and densities (n_i, n_e) in the edge pedestal region. A basic assumption for neoclassical theory is that the poloidal ion gyroradius ρ_i is significantly smaller than the gradient length L of the profiles ($\rho_i \ll L$). This condition is, however, not necessarily satisfied in the edge region of an H-mode plasma.

Moreover, because gradients of the input profiles are used in the bootstrap calculation, smooth pedestal profiles are needed. Therefore, edge measurements from, e.g., Thomson scattering (TS) or charge exchange recombination spectroscopy (CXRS) are typically fitted by a modified hyperbolic tangent function (mtanh) [5]. However, the mtanh function does not always lead to an acceptable fit to the data. For example in ASDEX Upgrade pedestal profiles are more accurately fitted with a piecewise linear function [6]. This means the result of the bootstrap calculation could depend on the choice of fit function.

Finally, the edge measurements need to have a high enough accuracy and radial resolution. Especially for the ion

temperature—measured by CXRS, which means the resolution is partly determined by the width of the neutral beam—this can be an issue. In such a case typically $T_i = T_e$ is assumed. Caution is, however, needed with this assumption, because at low collisionality $T_i = T_e$ is typically not valid in the pedestal region [7]. Another assumption often made due to the lack of an accurate measurement is $Z_{eff} = 1$. All assumptions made obviously also have an influence on the final result of the neoclassical determination of j_ϕ in the edge.

The reasons mentioned above call for an independent measurement of the edge j_ϕ that allows one to check the validity of the neoclassical calculation. Moreover, such a measurement would also allow one to find a complete, self-consistent set of edge profiles, that fit both density, temperature and j_ϕ measurements. When used as input to a stability analysis, this self-consistent set of edge profiles could in turn lead to a more accurate determination of the pedestal stability.

2. Measuring j_ϕ in the plasma edge

Motional Stark effect (MSE) diagnostics are routinely used in tokamaks to derive j_ϕ from the measured magnetic pitch angle $\gamma_m = \arctan(B_\theta/B_\phi)$, with B_θ the poloidal and B_ϕ the toroidal magnetic field [8]. Because γ_m depends on the integrated current, measuring a change of j_ϕ in the edge is difficult, as j_ϕ has to compete with the total plasma current in order to cause a noticeable change in γ_m. Moreover, MSE depends on the local radial electric field E_r as well, which can be large in the pedestal region during H-mode. Techniques other than MSE have been used for edge current measurements, but typically long integration times are necessary (~100 ms) [9]. A very recent method based on electron Bernstein wave emission looks promising in terms of spatial and time resolution, but requires complicated data analysis [10].

γ_m relates to j_ϕ through B_θ and Ampère's law. A change ΔB_θ due to a change in j_ϕ leads to following change in γ:

$$\Delta\gamma_m = \frac{B_\phi \Delta B_\theta}{B_\theta^2 + B_\phi^2}. \quad (1)$$

This means that in devices with a similar poloidal field B_θ but a lower toroidal field B_ϕ compared with conventional tokamaks, $\Delta\gamma_m$ will be larger and hence changes in the edge j_ϕ easier to detect. For the spherical tokamak MAST $B_\phi \approx 0.25$ T at the low field side edge, whereas $B_\theta \approx 0.2$ T. In a MAST H-mode a 10% bootstrap fraction is not unreasonable, which means an increase in $\Delta B_\theta \approx 0.02$ T over the pedestal. The resulting change in pitch angle according to (1) would thus be $\Delta\gamma_m \approx 3^\circ$. At 2 ms time resolution the MAST MSE system is capable of resolving this expected change in γ_m [11–13].

An MSE diagnostic does not measure γ_m directly, but instead measures a polarization angle γ that in the absence of a radial electric field E_r is proportional to γ_m. When E_r cannot be neglected, as is the case in the H-mode pedestal, a correction for E_r is necessary. When the MSE measurements are taken in the equatorial plane of the plasma, which is the case for the MAST discharge presented in this paper (#24409),

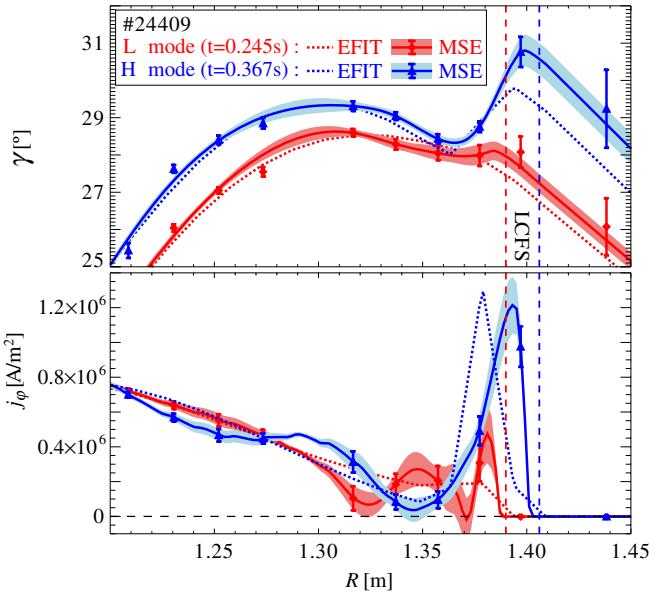

Figure 1. Profiles of γ and j_ϕ during L-mode and H-mode. The dotted lines are the result of an EFIT equilibrium reconstruction, the full lines with (shaded) error bars are MSE measurements of γ (top) and j_ϕ derived from γ directly using Ampère's law (bottom). In H-mode a clear peaking of γ and j_ϕ is observed in the edge.

$B_\theta = B_Z$ and the angle γ measured by the MSE diagnostic is

$$\tan(\gamma) = \frac{-\cos(\beta)B_Z - (E_r/v)\cos(\alpha+\beta)}{\sin(\alpha)B_\phi}, \quad (2)$$

where α is the angle between the toroidal direction and the neutral beam, β is the angle between the neutral beam and the line-of-sight and v is the beam velocity [8]. By using equation (2) to constrain the equilibrium reconstruction in codes such as EFIT B_Z and j_ϕ can be found [14]. However, when a strong pressure gradient is present, as is the case in H-mode, it is often difficult to find optimal settings for the basis functions used in EFIT. For the data shown in figure 1 splines were used as basis functions with eight knot points, mainly concentrated towards the edge of the plasma. This resulted in EFIT pressure and γ-profiles that followed the trend of the TS (for pressure) and MSE (for γ) data, but did not fit it perfectly. For γ this can be seen in figure 1. When the number of knot points was increased, unfortunately, EFIT no longer converged to a solution.

A more accurate result, including an estimate of the error, can be obtained by calculating B_Z directly from the MSE angle γ and then use Ampère's law to derive j_ϕ [15]:

$$\mu_0 j_\phi = \frac{\partial B_R}{\partial Z} - \frac{\partial B_Z}{\partial R}. \quad (3)$$

B_ϕ, E_r and $\partial B_R/\partial Z$ are unknowns in equations (2) and (3) and will be discussed below. Figure 1 shows profiles of γ and the corresponding j_ϕ in L- and H-mode, both from a MSE constrained EFIT reconstruction (dotted lines) and as derived from the MSE data directly (full lines with shaded error bars). Clearly an increase of γ near the last closed flux surface (LCFS) is observed for the H-mode phase, and consequently a peak in the edge current.

The value of B_ϕ needed in equation (2) is taken from an initial EFIT reconstruction. This can be done because B_ϕ is only weakly dependent on the local j_ϕ in the edge. An extra check on B_ϕ is that in the edge of the plasma it has to be close to the well-known vacuum toroidal field.

E_r is derived from the ion fluid as

$$E_r = -v_\phi \times B_Z + v_Z \times B_\phi + \frac{\nabla(n_\mathrm{i} T_\mathrm{i})}{e n_\mathrm{i}}, \qquad (4)$$

where v_ϕ and v_Z are the toroidal and poloidal plasma rotation and T_i and n_i are the ion temperature and density. In this discharge T_i and v_ϕ are measured with CXRS and n_i is assumed to be equal to the electron density n_e measured with TS [16, 17]. No measurement of v_Z exists for this discharge, but it was observed in other discharges that v_Z is, even in H-mode, an order of magnitude lower than v_ϕ [18]. With B_ϕ being of the order of B_Z at the low-field side edge of the MAST tokamak, the term $v_Z \times B_\phi$ can be neglected with respect to the $v_\phi \times B_Z$ term.

In the plasma edge the spatial resolution of the CXRS diagnostic is insufficient to calculate $\nabla(n_\mathrm{e} T_\mathrm{i})$. Here the assumption $T_\mathrm{i} = T_\mathrm{e}$ was made. In the first plot of figure 2 measurements of both T_e from TS and T_i from CXRS are shown. For the discharge under investigation the assumption $T_\mathrm{i} = T_\mathrm{e}$ in the plasma edge is justified. With the above assumptions (4) becomes

$$E_r = -v_\phi \times B_Z + \frac{\nabla(n_\mathrm{e} T_\mathrm{e})}{e n_\mathrm{e}}. \qquad (5)$$

To calculate E_r the measurement data were fitted with a mtanh function over the pedestal (normalized poloidal flux $\psi > 0.7$) continuously connected to a spline fit of the core data. Except for v_ϕ, that shows no evidence of a pedestal-like profile and was fitted with a spline only. The fits to the measurement data of T_e, n_e and v_ϕ are shown as full lines in the top three plots of figure 2.

Solving (5) and (2) returns E_r and B_Z. The full line in the fourth plot of figure 2 shows the calculated E_r. In the same plot an independent measurement of E_r in the plasma edge is shown (crosses). These measurements were obtained from Doppler spectroscopy measurements on He^+ injected into the plasma edge [19]. The resulting E_r is of the same amplitude but its profile is wider than the E_r profile based on TS and CXRS measurements. A wide, flat E_r profile, however, results in a shift of B_Z (see (2)), but does not change the gradient of the B_Z profile and hence has little influence on j_ϕ (see (3)). This means that using the E_r based on TS and CXRS measurements, if anything, the effect of E_r is overestimated. Nonetheless, even this overestimated effect on B_Z and j_ϕ is very small. This can be seen in the bottom two plots of figure 2 where the B_Z and j_ϕ profiles both with and without E_r correction are shown. Uncertainties in the determination of E_r are therefore not considered a major point of concern at MAST.

Finally the term $\partial B_R/\partial Z$ in Amperè's law can be found from the initial EFIT reconstruction. Taking into account that the flux surface shape depends only weakly on the local j_ϕ, it

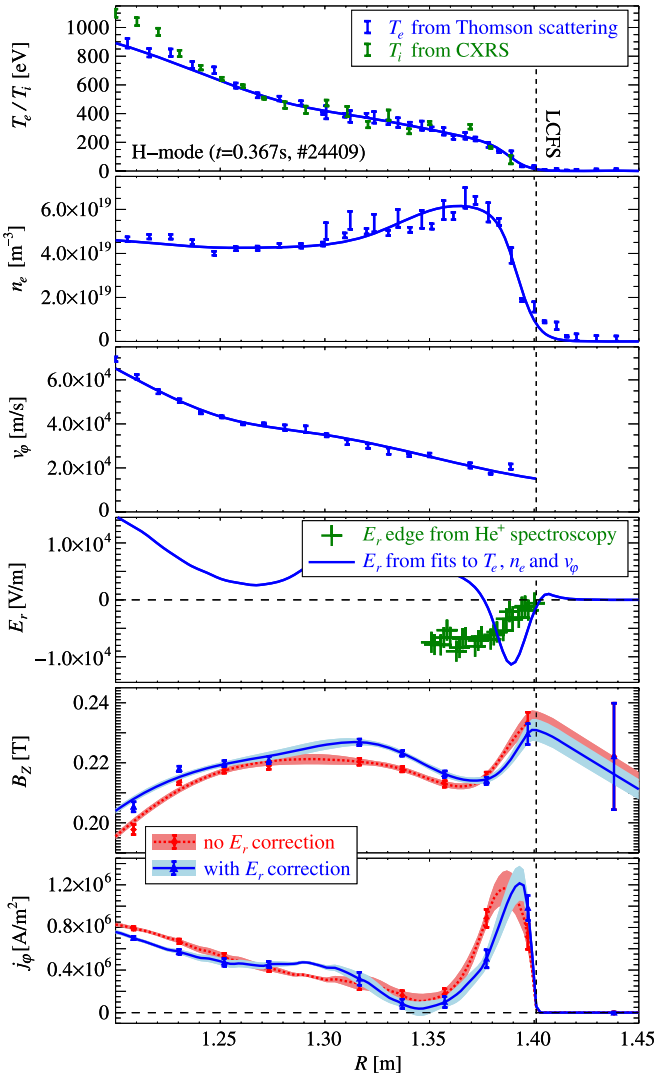

Figure 2. The top plot shows measurements of T_i by CXRS and T_e by TS, plus a fit to T_e. It is observed that, for this discharge, $T_\mathrm{i} = T_\mathrm{e}$ in the plasma edge. The second plot shows n_e measurements by TS and the fitted profile. The third plot shows v_ϕ measurements by CXRS and again the fitted profile. The fourth plot shows the E_r based on T_e, n_e and v_ϕ (full line). This is the E_r profile used for correcting the MSE measurements. As a comparison also a He^+ spectroscopic measurement for the edge E_r is given (crosses), which is of the same order, but has a broader profile in the edge. This means that the E_r used for the MSE correction is possibly an overestimate. The fifth and sixth plot, that show B_Z and j_ϕ with and without E_r correction, indicate that, even with a possibly overestimated E_r, the correction is only small.

can be assumed that: $B_R/B_Z \approx B_R^{\mathrm{EFIT}}/B_Z^{\mathrm{EFIT}}$. Deriving left and right hand terms to Z one finds

$$\frac{\partial B_R}{\partial Z} = \frac{B_Z}{B_Z^{\mathrm{EFIT}}} \frac{\partial B_R^{\mathrm{EFIT}}}{\partial Z}. \qquad (6)$$

B_Z can be calculated for every MSE channel and its error can be derived from the measurement error in γ. The data points with error bars in the fifth plot of figure 2 indicate this. However, for the gradient of B_Z needed in (3) the spatial resolution of the MSE diagnostic is very coarse. Therefore, smooth γ-profiles were obtained by fitting a spline to the

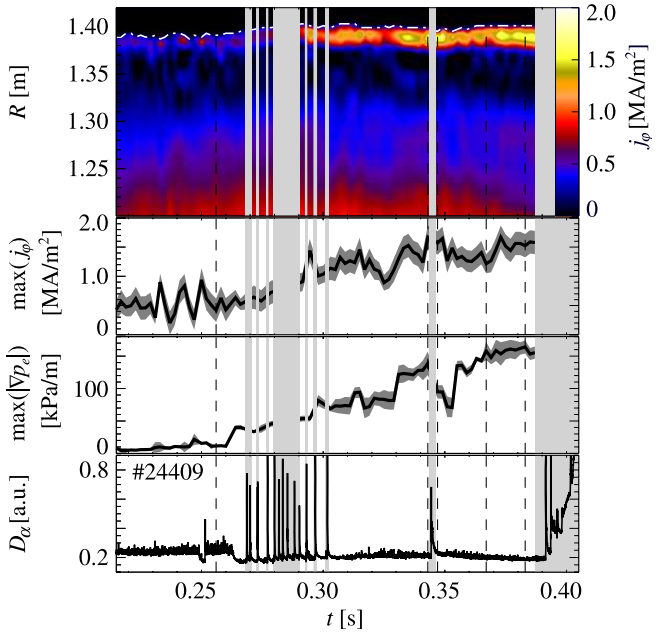

Figure 3. The evolution of j_ϕ, max(j_ϕ), max(|∇p_e|) and the D_α emission. The position of the LCFS is indicated in the contour plot by the white —· line. The vertical dashed lines indicate the profiles shown in figures 1, 2 and 4.

measured γ. These smooth γ-profiles were then used to calculate smooth B_Z and j_ϕ profiles using equations (2), (3) and (5), indicated by the full lines in the bottom two plots of figure 2.

In the introduction it was stated that the fitting of the pedestal T_i, T_e and n_e-profiles, and particularly the choice of fit function, could possibly affect the calculated bootstrap current. Of course the same holds here for fitting the MSE data points to derive j_ϕ. Therefore, we will estimate the error of the fitting. To do so, a set of splines was fitted to the measured γ perturbed by its errors. For each perturbed spline B_Z and j_ϕ were calculated and the rms determines the error. This is indicated by the shaded areas around the profiles shown in figures 1, 2 (bottom two plots), 3 and 4.

3. The evolution of j_ϕ in the plasma edge

Figure 3 shows the evolution of j_ϕ, max(j_ϕ), max(|∇p_e|) and the D_α emission during the discharge. The periods around the ELMs are blocked by grey areas because no reliable MSE measurement exists at those times.

The L–H transition into a high frequency, type III ELMy H-mode occurs at $t = 0.263$ s. Apart from one outlier at $t = 0.295$ s the edge j_ϕ gradually increases during this type III phase and so does max(|∇p_e|). This is consistent with the picture of pressure driven edge current. However, due to the short inter-ELM period typically only one j_ϕ profile can be obtained per ELM period. Hence, no information can be obtained about the inter-ELM evolution of j_ϕ.

The focus of the following discussion therefore lies on the two long ELM-free periods following the type III phase: starting at $t = 0.303$ s and separated by a type I ELM at $t = 0.345$ s. A final ELM at $t = 0.392$ s terminates the H-mode, quickly followed by a disruption.

During these ELM-free periods strong currents are observed in the plasma edge. The edge current is located at the pedestal position, about 2–3 cm inside the LCFS. The amplitude of the edge j_ϕ reaches up to 1.6 MA m^{-2}, which is of the order of the central current density.

On average max(j_ϕ) increases with increasing max(|∇p_e|). However, the changes in max(j_ϕ) are less abrupt than those in max(|∇p_e|) and are delayed several milliseconds with respect to the changes in max(|∇p_e|) . Two examples of this are the following.

- The sudden increase in max(|∇p_e|) at $t = 0.329$ s is accompanied by a much more gradual increase in max(j_ϕ).
- At the ELM crash ($t = 0.345$ s) max(|∇p_e|) drops significantly whereas max(j_ϕ) remains high for ~4 ms (up to $t = 0.349$ s), after which it only decreases gradually.

Other interesting observations are the decrease in max(j_ϕ) in periods where max(|∇p_e|) remains more or less constant. This happens from $t = 0.317$ s to $t = 0.327$ s, and again from $t = 0.335$ s to $t = 0.341$ s (just before the ELM).

The delays and more gradual evolution of j_ϕ suggest that current diffusion plays an important role. Another influence could be the collisionality [20]. This is because the pedestal pressure in MAST is strongly dominated by the density (see figure 2). In the next section both will be investigated.

4. Comparison with neoclassical bootstrap calculation and current diffusion

The edge j_ϕ during H-mode is typically attributed to the high bootstrap current fraction due to the large pressure gradient. In the previous section it was shown that indeed the measured j_ϕ on average increases with increasing ∇p_e. For a more detailed comparison, however, a full neoclassical calculation needs to be done.

In such a full calculation the current comes from the bootstrap drive, including the effect of collisionality, but also the inductively driven part, because the pedestal profiles also change the resistivity. Finally the calculated current has to be part of a self-consistent equilibrium.

Two codes were used to calculate the edge j_ϕ based on the profiles of T_e, T_i and n_e. Again $T_i = T_e$ was assumed for the pedestal and $Z_{eff} = 1$ was assumed over the whole plasma.

The first code used is the HELENA equilibrium code, where the formulae of [3, 4] are implemented for the bootstrap calculation [21]. HELENA treats every time frame separately and therefore does not include current diffusion.

The second code is the CRONOS suite [22]. This suite of codes also uses HELENA for the equilibrium, but calculates the bootstrap current drive with NCLASS [23]. Furthermore, the CRONOS suite does include the current diffusion calculation.

The top plots of figure 4 shows a comparison between j_ϕ derived from MSE and j_ϕ calculated by HELENA and CRONOS for three time points: just before the ELM ($t =$

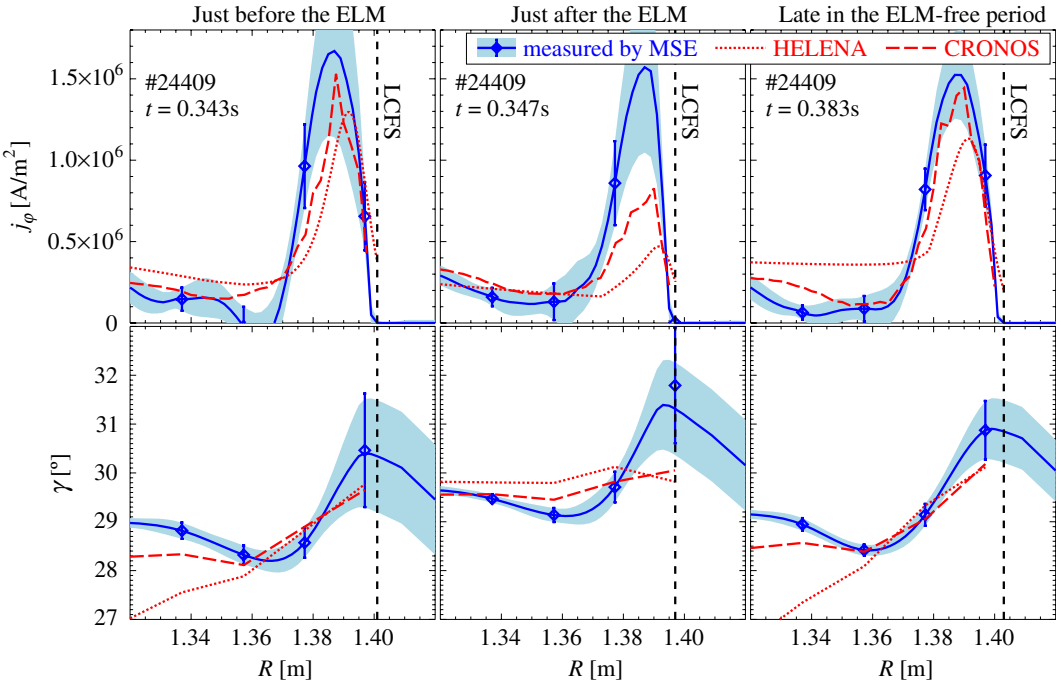

Figure 4. Comparison of the neoclassical calculation, with (CRONOS) and without (HELENA) current diffusion, and the MSE measurement of γ (bottom) and j_ϕ (top). Just before the ELM and late in the ELM-free period reasonable agreement is found between the calculations and the measurement. Just after the ELM the calculations predict significantly less edge current than that measured. The CRONOS calculation, that included current diffusion, shows, however, a higher current than the HELENA calculation without current diffusion. This indicates current diffusion seems to be an important factor.

0.343 s), just after the ELM ($t = 0.347$ s) and late in the ELM-free period ($t = 0.383$ s).

Although calculating j_ϕ directly from MSE is useful because one can immediately see the evolution of relevant physical parameter (being j_ϕ), for comparing with neoclassical calculation it is less ideal. Mainly because one is then comparing one derived quantity—j_ϕ calculated using neoclassical theory and the n_e, T_e and T_i input profiles—with another—j_ϕ derived from fits to and derivatives of the MSE data. It is much better to be able to compare with raw measurements directly.

Thanks to the fact that both HELENA and CRONOS return the complete equilibrium, hence profiles of B_Z and B_ϕ, and that their input profiles uniquely define E_r equations (2) and (5) can be used to calculate the expected MSE angles γ_{HELENA} and γ_{CRONOS}. These can then be directly compared with the raw γ-profiles measured by MSE. This more straightforward comparison is shown in the lower plots of figure 4. Because no fitting to the MSE data is required for this direct comparison, and hence no errors due to the fitting are introduced, the lower plots of figure 4 are the most relevant in comparing the neoclassical calculation with the MSE measurement.

One observes that just before the ELM and long after the ELM both the HELENA and the CRONOS calculations are in good agreement with the measurements. CRONOS also gives better agreement in the core of the plasma (not shown in the figure).

Just after the ELM, however, the agreement is worse, especially for the HELENA code. The inclusion of current diffusion in CRONOS does lead to a higher current, but not enough to agree with the MSE measurement. This suggests that current diffusion probably is a key factor, but also indicates that the actual current diffusion is slower than neoclassical theory predicts. In other words, the neoclassical resistivity seems very large. This has been observed in previous experiments on current diffusion as well, where it was suggested that Spitzer resistivity agrees better with the experimental evidence [24, 25].

Just before the ELM and late in the second ELM-free period both HELENA and CRONOS give the same result for γ in the edge, indicating that by then the edge current is fully relaxed. Despite agreeing within the error bars with the measured γ, the gradients of γ_{HELENA} and γ_{CRONOS}, and hence the calculated currents, are even at these times slightly lower than measured ones. This is the case throughout the discharge. Possible reasons for this difference could be the following.

- The fact that neoclassical theory is not fully valid, because $\rho_i \gg L$ in the H-mode edge.
- Certain elements that are not included in the neoclassical model, such as the enhancement of the bootstrap current due to E_r [26].
- The fact that the functions fitted to the T_i, T_e and n_e measurements do not describe the pedestal profiles accurately enough.

The latter means that, by e.g. integrated data analysis [27, 28], it would be possible to find pedestal profiles that fit the measured T_i, T_e, n_e and γ simultaneously. For example, the gradients of T_i, T_e and n_e need only to be of order 5% to 10% higher, which will increase both E_r and the bootstrap

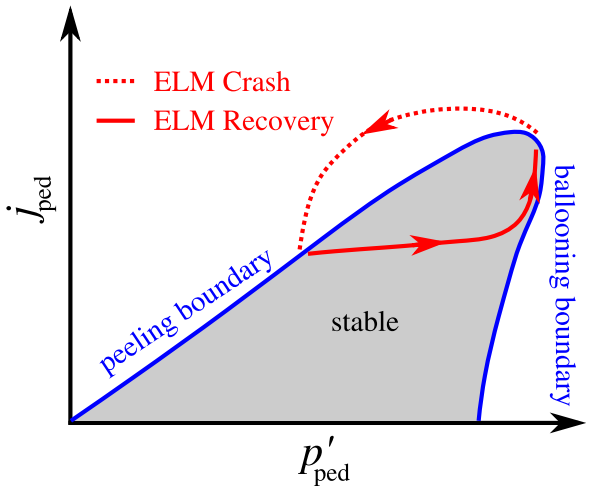

Figure 5. Simplified model of the type I ELM cycle according to the peeling–ballooning model. The pressure gradient builds up until the ballooning boundary is reached. The pedestal current can then still rise due to current diffusion until also the peeling boundary is reached. At that point the peeling–ballooning mode is destabilized and the ELM crash occurs (figure adapted from [29]).

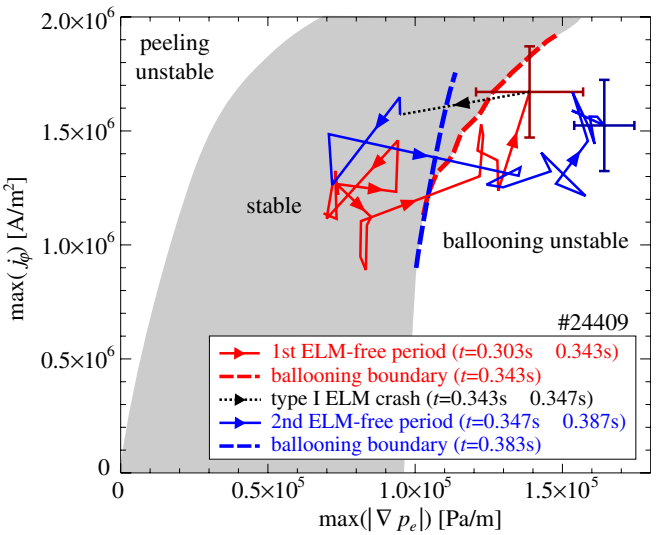

Figure 6. max(j_ϕ) is plotted versus max(|∇p_e|) showing the stability evolution. The ballooning boundary (thick, dashed lines) was calculated using ELITE at $t = 0.343$ s and $t = 0.383$ s. For these time frames also the errors of max(j_ϕ) and max(|∇p_e|) are indicated (error bars are of similar size for the other data points). The peeling boundary of the stable region (top left) is indicative only as no unstable peeling modes were found in the vicinity of the data points at $t = 0.343$ s or $t = 0.383$ s.

current, in order to get good agreement with the raw MSE γ angles. Moreover, T_i, T_e and n_e profiles with a 5% to 10% increase in pedestal gradient, compared with the ideal mtanh fit, would still be in good agreement with the TS and CXRS measurements. Such profiles could then possibly give a better and self-consistent description of the pedestal. When using these profiles as an input to stability analysis, more reliable results could possibly be obtained.

5. Notes on stability

The stability of the H-mode pedestal with respect to ELMs can be described by the peeling–ballooning model [29]. It describes a stability region in terms of the pedestal pressure gradient p'_{ped} and current j_{ped}. A simplified picture of the model is shown in figure 5 (figure adapted from [29]). If the pressure gradient exceeds a certain threshold ballooning modes are destabilized (the ballooning boundary). The pedestal current density j_{ped}, however, reduces the edge magnetic shear, which in turn stabilizes the ballooning modes and shifts the ballooning boundary to higher values of p'_{ped}. On the other hand increasing j_{ped} will provide free energy that can destabilize peeling modes (the peeling boundary). When crossing the threshold at both high p'_{ped} and high j_{ped}, where the peeling and ballooning boundaries meet, coupled peeling–ballooning modes are destabilized.

Figure 5 also illustrates schematically a type I ELM cycle: p'_{ped} increases during the inter-ELM period and saturates near the ballooning boundary. j_{ped} also rises, but more slowly due to current diffusion. This means j_{ped} still grows when p'_{ped} has already fully recovered. At high enough j_{ped} the stability boundary is then crossed and peeling–ballooning modes destabilized, leading to the ELM crash.

However, detailed study at ASDEX Upgrade of the inter-ELM evolution of n_e and T_e profiles showed that the slow build-up of the derived edge j_ϕ found from neoclassical current diffusion calculations cannot explain the gap between the saturation of max(|∇p_e|) and the onset of the ELM [30]. Again a possible explanation could be that the actual current diffusion is slower than neoclassically calculated (see previous section). However, in the MAST discharge presented in this paper both the measured max(|∇p_e|) and the measured max(j_ϕ) are saturated well before the ELM, especially near the end of the second ELM-free period from $t = 0.375$ s until the end of the measurements at $t = 0.387$ s. This can be seen in figure 3. Unfortunately the neutral beam switched off before the ELM at $t = 0.392$ s that terminates the H-mode and the discharge, such that no MSE measurements exist for the remaining 5 ms up to the ELM. We can therefore not state with certainty that the saturation of max(j_ϕ) and max(|∇p_e|) that is seen from $t = 0.375$ s until $t = 0.387$ s persists until $t = 0.392$ s. We assume, however, it does.

In figure 6 the measured max(j_ϕ) is plotted against the measured max(|∇p_e|). i.e. the experimental version of the simplified stability plot of figure 5. Ideally a stability analysis should be performed for every data point in the figure. This, however, falls out of the scope of this paper. Therefore, a stability analysis was done only for the time frames at $t = 0.343$ s (just before the ELM) and $t = 0.383$ s (near the end of the discharge). The stability calculations were done for toroidal mode numbers 5-30 using the ELITE code [31, 29].

At $t = 0.343$ s the plasma is found to be marginally unstable against ballooning modes. The calculated stability boundary, indicated by the red dashed line in figure 6, lies within the error bars of the data point. During the first ELM-free period, i.e. up to $t = 0.343$ s, the (max(|∇p_e|), max(j_ϕ)) data points evolve more or less along the ballooning boundary towards higher max(j_ϕ); in agreement with the peeling–ballooning model. The only caveat is that at the ELM-crash

only ballooning modes, rather than peeling–ballooning modes, are found to be unstable.

At $t = 0.383$ s both $\max(|\nabla p_e|)$ and $\max(j_\phi)$ are saturated. This saturation starts at $t = 0.375$ s and lasts at least until the end of the measurements at $t = 0.387$ s. It is assumed this saturation continues up to the ELM at $t = 0.392$ s, although no MSE measurements were available anymore from $t = 0.387$ s up to $t = 0.392$ s (see above). It is, however, clear that at $t = 0.383$ s the plasma is (at least marginally) stable, because the ELM only occurs more than 8 ms later. The ELITE stability analysis, however, predicts that, with the measured $\max(|\nabla p_e|)$ and $\max(j_\phi)$ at $t = 0.383$ s, the plasma should be strongly unstable against ballooning modes. Moreover, the corresponding calculated stability boundary, indicated by the blue dashed line in figure 6, lies well outside the error bars of the data point. This indicates that in this case crossing the static stability boundary does not predict the ELM crash.

Because the calculated stability depends strongly on both the shape of the plasma cross section, as well as on the pressure and current profiles, it is possible that the profiles used do not accurately enough describe the pedestal. This could lead to a false prediction on the stability. Again this calls for an accurate, self-consistent description of the pedestal profiles that fits the measurements of T_i, T_e, n_e and γ.

6. Summary and conclusion

Both bootstrap current and stability calculations depend strongly on the quality of and assumptions on the input profiles. Independent measurements of the current in the plasma edge could allow for a better description of the plasma pedestal, a validation of neoclassical bootstrap current and finally a more accurate determination of the stability with respect to ELMs.

Thanks to a large pitch angle and a small E_r correction, MSE can be used as a tool for routinely measuring the edge j_ϕ evolution in spherical tokamaks. First measurements show that neoclassical calculations approximately agree with measurements when the edge current is fully relaxed. Just after the ELM event, however, the current remains high for several milliseconds. This is longer than what is found from current diffusion calculations using neoclassical resistivity.

The evolution of j_ϕ and ∇p_e in a stability plot shows that both j_ϕ and ∇p_e can be fully relaxed well before the ELM crash. This does not agree with the hypothesis that ∇p_e can only be saturated before the ELM onset as long as j_ϕ still rises (e.g. due to current diffusion). Preliminary stability analysis also indicates that the plasma crosses the stability boundary well before the ELM crash.

Further work needs to be done, e.g. by integrated data analysis, on determining pedestal profiles that fit both the measured T_i, T_e, n_e profiles and the measured γ-profiles for MSE. Such profiles could then possibly give a better and self-consistent description of the pedestal. Furthermore, when using these profiles as an input to stability analysis, more reliable results could possibly be obtained.

Acknowledgments

This work was jointly funded by the RCUK Energy programme under grant EP/I501045 and the European Communities under the Contract of Association between EURATOM and CCFE. The views and opinions expressed herein do not necessarily reflect those of the European Commission.

References

[1] Evans T E *et al* 2004 Suppression of large edge-localized modes in high-confinement DIII-D plasmas with a stochastic magnetic boundary *Phys. Rev. Lett.* **92** 235003

[2] Lang P T *et al* and the ASDEX Upgrade Team 2003 ELM frequency control by continuous small pellet injection in ASDEX Upgrade *Nucl. Fusion* **43** 1110

[3] Sauter O, Angioni C and Lin-Liu Y R 1999 Neoclassical conductivity and bootstrap current formulas for general axisymmetric equilibria and arbitrary collisionality regime *Phys. Plasmas* **6** 2834

[4] Sauter O, Angioni C and Lin-Liu Y R 1999 Erratum: Neoclassical conductivity and bootstrap current formulas for general axisymmetric equilibria and arbitrary collisionality regime [Phys. Plasmas 6, 2834 (1999)] *Phys. Plasmas* **9** 5140

[5] Groebner R J, Mahdavi M A, Leonard A W, Osborne T H and Porter G D 2002 Role of neutrals in density pedestal formation in DIII-D *Plasma Phys. Control. Fusion* **44** A265

[6] Schneider P A, Wolfrum E, Kurzan B and Zohm H 2010 Alternative method for characterization of inter-ELM edge profiles of type I ELMy H-modes in ASDEX Upgrade *37th EPS Conf. on Controlled Fusion and Plasma Physics (EPS) (Dublin, Ireland)* P-2.157

[7] Morgan T, Meyer H, Temple D and Tallents G 2010 A new edge ion temperature measurement diagnostic on the MAST tokamak *37th EPS Conf. on Controlled Fusion and Plasma Physics (EPS) (Dublin, Ireland)* P-5.122

[8] Levinton F M, Gammel G M, Kaita R, Kugel H W and Roberts D W 1990 Magnetic field pitch angle diagnostic using the motional Stark effect (invited) *Rev. Sci. Instrum.* **61** 2914

[9] Thomas D M, Leonard A W, Lao L L, Osborne T H, Mueller H W and Finkenthal D K 2004 Measurement of pressure-gradient-driven currents in tokamak edge plasmas *Phys. Rev. Lett.* **93** 065003

[10] Shevchenko V F, De Bock M F M, Freethy S J, Saveliev A N and Vann R G L 2011 Two-dimensional studies of electron Bernstein wave emission in MAST *Fusion Sci. Technol.* **59** 663

[11] de Bock M F M, Conway N J, Walsh M J, Carolan P G, Hawkes N C and the MAST Team 2008 *Ab initio* modeling of the motional stark effect on MAST *Rev. Sci. Instrum.* **79** 10F524

[12] De Bock M F M, Michael C A, Conway N J, Appel L, Chapman I T, Gryaznevich M, Tojo H and Turnyanskiy M R 2009 First multi-chord MSE measurements on MAST *36th EPS Conf. on Controlled Fusion and Plasma Physics (Sofia, Bulgaria)* vol 33E (ECA) P-5.186

[13] Conway N J, De Bock M F M, Michael C A, Walsh M J, Carolan P G, Hawkes N C, Rachlew E, McCone J F G, Shibaev S and Wearing G 2010 The MAST motional Stark effect diagnostic *Rev. Sci. Instrum.* **81** 10D738

[14] Appel L C, Huysmans G T A, Lao L L, McCarthy P J, Muir D G, Solano E R, Storrs J, Taylor D, Zwingmann W and contributors to the EFDA Integrated Tokamak Modelling (ITM) Task Force and JET-EFDA Contributors

2006 A unified approach to equilibrium reconstruction *33rd EPS Conf. on Controlled Fusion and Plasma Physics (Rome, Italy)* vol 30C (ECA) P-2.184

[15] Petty C C, Lin-Liu Y R, Luce T C, Makowski M A, Prater R, Schuster D I, St. John H E and Wong K L 2001 Localized measurements of electron cyclotron current drive using MSE spectroscopy on the DIII-D tokamak *Nucl. Fusion* **41** 551

[16] Conway N J, Carolan P G, McCone J, Walsh M J and Wisse M 2006 High-throughput charge exchange recombination spectroscopy system on MAST *Rev. Sci. Instrum.* **77** 10F131

[17] Scannell R, Walsh M J, Dunstan M R, Figueiredo J, Naylor G, O'GormanT, Shibaev S, Gibson K J and Wilson H 2010 A 130 point Nd:YAG Thomson scattering diagnostic on MAST *Rev. Sci. Instrum.* **81** 10D520

[18] Field A R, McCone J, Conway N J, Dunstan M, Newton S and M Wisse 2009 Comparison of measured poloidal rotation in MAST spherical tokamak plasmas with neo-classical predictions *Plasma Phys. Control. Fusion* **51** 105002

[19] Meyer H, Bunting C, Carolan P G, Conway N J, Dunstan M R, Kirk A, Scannell R, Temple D, Walsh M and the MAST and NBI Teams 2008 The structure, evolution and role of the radial edge electric field in H-mode and L-mode on MAST *J. Phys.: Conf. Ser.* **123** 012005

[20] Thomas D M, Leonard A W, Osborne T H, Groebner R J, West W P and Burrell K H 2006 The effect of plasma collisionality on pedestal current density formation in DIII-D *Plasma Phys. Control. Fusion* **48** A183–91

[21] Huysmans G T A, Goedbloed J P and Kerner W O K 1991 *Proc. CP90 Europhysics Conf. on Computational Physics (10–13 September 1990, Amsterdam, The Netherlands)* (Singapore: World Scientific) p371

[22] Artaud J F *et al* 2010 The CRONOS suite of codes for integrated tokamak modelling *Nucl. Fusion* **50** 043001

[23] Houlberg W A, Shaing K C, Hirshman S P and Zarnstorff M C 1997 Bootstrap current and neoclassical transport in tokamaks of arbitrary collisionality and aspect ratio *Phys. Plasmas* **4** 3230

[24] Jenkins I, Baruzzo M, Brix M, Challis C D, Hawkes N C, Litaudon X, Mailloux J, Rimini F G, de Vries P C and JET-EFDA Contributors 2010 Test of current ramp modelling for AT regimes in JET *37th EPS Conf. on Controlled Fusion and Plasma Physics (EPS) (Dublin, Ireland)* P-2.178

[25] Keeling D D, Akers R J, De Bock M F M, Challis C D, Michael C A, Patel A and the MAST team 2011 Test of current diffusion modelling in MAST current ramp-up *38th EPS Conf. on Controlled Fusion and Plasma Physics (EPS) (Strasbourg, France)* P-2.178

[26] Kagan G and Catto P J 2010 Enhancement of the bootstrap current in a tokamak pedestal. *Phys. Rev. Lett.* **105** 045002

[27] Fischer R, Dinklage A A and Pasch E 2003 Bayesian modelling of fusion diagnostics *Plasma Phys. Control. Fusion* **45** 1095

[28] Svensson J *et al* and JET-EFDA Contributors 2010 Connecting physics models and diagnostic data using bayesian graphical models *37th EPS Conf. on Controlled Fusion and Plasma Physics (Dublin, Ireland)* vol 30C (ECA) O4.117

[29] Snyder P B, Wilson H R, Ferron J R, Lao L L, Leonard A W, Osborne T H, Turnbull A D, Mossessian D, Murakami M and Xu X Q 2002 Edge localized modes and the pedestal: A model based on coupled peeling–ballooning modes *Phys. Plasmas* **9** 2037

[30] Bruckhart A, Wolfrum E E, Fischer R, Lackner K, Zohm H and the ASDEX Upgrade Team 2010 Inter-ELM behaviour of the electron densitiy and temperature pedestal in ASDEX Upgrade *Plasma Phys. Control. Fusion* **52** 105010

[31] Wilson H R, Snyder P B, Huysmans G T A and Miller R L 2002 Numerical studies of edge localized instabilities in tokamaks *Phys. Plasmas* **9** 1277